Volume 5 | Number 6 | 14 February 2017 | Pages 1263–1556

Journal of Materials Chemistry C

Materials for optical, magnetic and electronic devices

rsc.li/materials-c

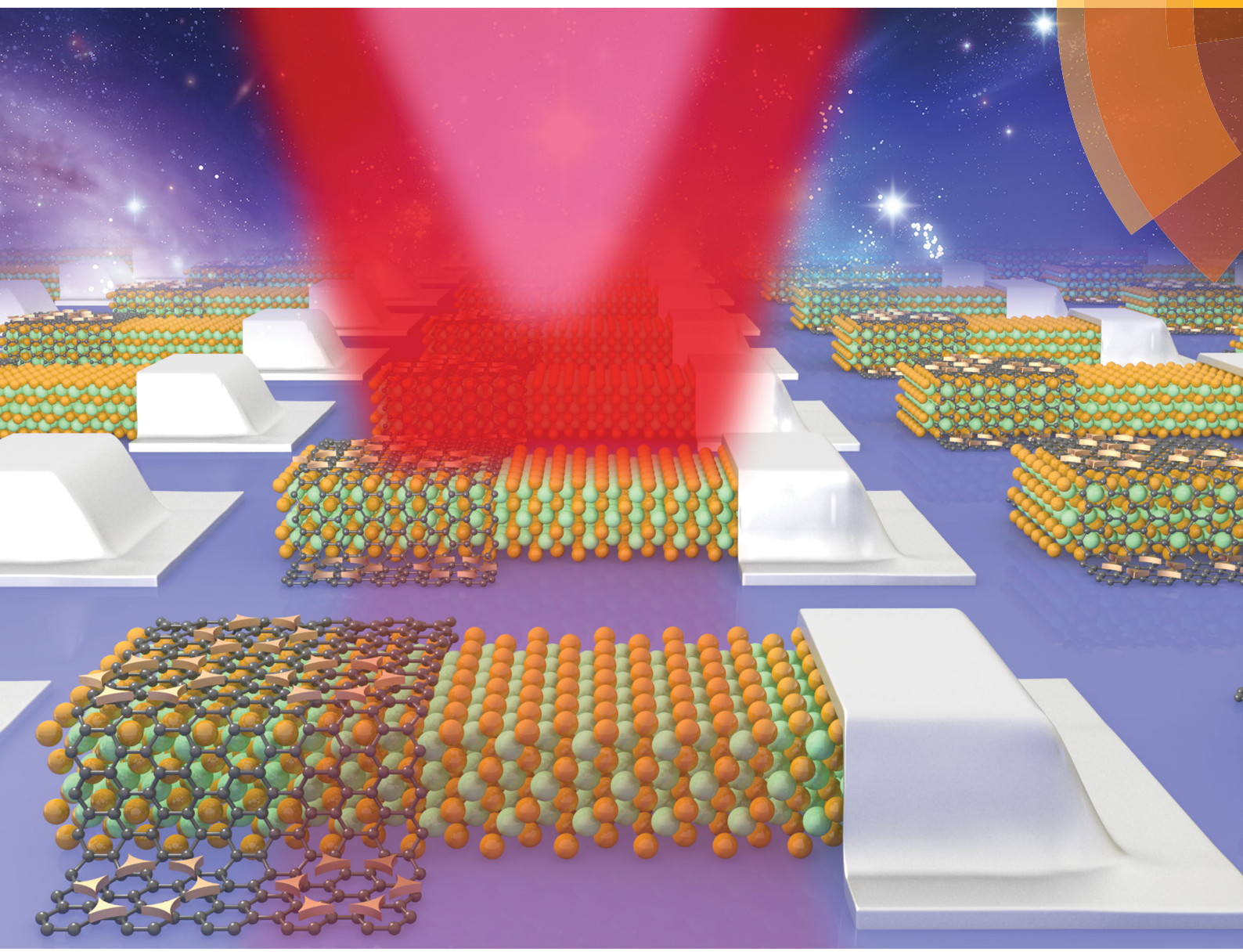

ISSN 2050-7526

ROYAL SOCIETY OF CHEMISTRY

PAPER

Lin-Bao Luo *et al.*

A sensitive red light nano-photodetector propelled by plasmonic copper nanoparticles

Journal of Materials Chemistry C

PAPER

View Article Online
View Journal | View Issue

Cite this: J. Mater. Chem. C, 2017, 5, 1328

A sensitive red light nano-photodetector propelled by plasmonic copper nanoparticles†

Dan-Dan Wang, Cai-Wang Ge, Guo-An Wu, Zhi-Peng Li, Jiu-Zhen Wang, Teng-Fei Zhang, Yong-Qiang Yu and Lin-Bao Luo*

Received 25th November 2016,
Accepted 21st December 2016

DOI: 10.1039/c6tc05117k

www.rsc.org/MaterialsC

Plasmonic optoelectronic device based non-noble metal nanostructures (*e.g.* Al, In, *etc.*) have recently received increasing research interest due to their relatively low fabrication cost and tunable plasmon wavelength. In this study, we present a new plasmonic red light nano-photodetector by decorating a multi-layer graphene (MLG)–CdSe nanoribbon (CdSeNR) Schottky junction with a highly ordered plasmonic copper nanoparticle (CuNP) array, which exhibited obvious localized surface plasmon resonance in the range of 700–900 nm. Optoelectronic analysis reveals that the device metrics including the switch ratio, the responsivity and the detectivity considerably increased after functionalization with plasmonic CuNPs. Moreover, the response speed was fastened by nearly one order of magnitude. The observed optimization in device performance, according to theoretical simulations based on the finite element method (FEM) and experimental analysis, could be attributed to localized surface plasmon resonance (LSPR) induced hot electron injection. The above results signify that the present plasmonic CuNPs are equally important candidates for boosting the device performance of nano-optoelectronic devices.

1. Introduction

Surface plasmon resonance (SPR) is known to be the collective charge density oscillation that usually exists at the interfaces composed of two different media with opposite dielectric constants, for instance, a noble metal (NM) and dielectric.[1,2] Unlike the propagation of surface plasmon polaritons at a dielectric–metal interface, localized SPR (LSPR) normally on noble metal nanomaterials (*e.g.* Au and Ag) can cause sharp spectral absorption due to strong localized field enhancement and enhanced scattering.[3,4] It has been widely reported that the combination of plasmonic nanostructures with semiconductors offers a feasible route to improve the device performance of various optoelectronic devices.[5] Take a Schottky junction based solar cell for example, when plasmonic NM nanostructures were introduced into the device geometry, the strong near field around metal nanomaterials can be coupled to the nearby absorber layer and therefore increases its absorption.[6] In addition, the high local electromagnetic field can generate energetic electron–hole pairs, which may surmount the potential barriers, leading to efficient hot injection from the plasmonic material to the semiconductor, therefore contributing to photocurrent.[7,8] By this token, NM nanoparticles have been widely employed to boost the performance of a number of optoelectronic devices including photovoltaic devices,[9,10] photodetectors,[11,12] waveguides,[13] and so on.

As alternatives to conventional NM nanoparticles, poor metal nanoparticles (PM, *e.g.* Cu, In, Al, *etc.*) have been receiving an increasing amount of interest in that these metals have large negative real and small imaginary dielectric functions and therefore they can induce localized surface plasmon resonance (LSPR) as well.[14–16] Compared to NM nanoparticles, the plasmonic nanomaterials based on PM are advantageous not only for their relatively cheap cost as a result of their rich abundance in the Earth, but also for the widened electromagnetic spectrum.[17] Despite the obvious merits of plasmonic PM mentioned above, there is scarcity of investigation on the application of plasmonic PMs in semiconductor optoelectronics, the device performance of which can be optimized by NM nanoparticles.[18,19] Herein, we present the fabrication of plasmonic copper nanoparticles (CuNPs) for optimizing the sensitivity of the graphene–CdSe nanoribbon (CdSeNR) Schottky junction nano-photodetector. Device analysis reveals that when modified by CuNPs with apparent LSPR, the CuNP@graphene–CdSeNR Schottky junction device exhibits high sensitivity to 780 nm light illumination with good reproducibility. The corresponding device parameters in terms of responsivity and detectivity are higher than those of the device without modification. Such an optimization in device performance, according to our theoretical simulations, is due to the LSPR induced hot electron injection mechanism. This study suggests that plasmonic PM nanomaterials are equally efficient candidates for boosting the device performance of optoelectronic devices and systems.

School of Electronic Science and Applied Physics, Hefei University of Technology, Hefei, Anhui 230009, P. R. China. E-mail: luolb@hfut.edu.cn

† Electronic supplementary information (ESI) available. See DOI: 10.1039/c6tc05117k

2. Results and discussion

The plasmonic nanophotodetector was composed of individual CdSeNRs and graphene layers which were modified by plasmonic copper nanoparticles [Fig. 1(a)]. Raman analysis of the graphene in the ESI† reveals a weak D band (Fig. S1), and two strong bands with an intensity ratio less than 2 (I_G/I_{2D} = 1.6), indicative of the multi-layer feature.[20] To form an *Ohmic* contact with the CdSeNR, indium metal with a thickness of 100 nm was coated on the one hand of the NR by thermal evaporation [Fig. 1(b)]. As shown by the flow chart in Fig. 1(c), the hexagonal CuNPs were functionalized on the MLG film by a polystyrene (PS) nanosphere alignment assisted approach, followed by the deposition of a 12 nm thick Cu thin film through electron beam evaporation. The scanning electron microscopy (SEM) images in Fig. 1(d and e) show the morphology of the CuNPs at both low and high magnifications, respectively. It is clear that the MLG films were coated with a triangle-like CuNP array which was arranged in a hexagonal fashion, with nearly identical distances. The side length of the CuNPs is in the range of 120–170 nm, with an average value of about 145 nm. The CdSeNRs were synthesized by a conventional thermal evaporation method. From the corresponding SEM image shown in Fig. 1(f), one can see that the majority of product was composed of ribbon-like nanostructures. According to the energy dispersive spectroscopy (EDS) analysis (see Fig. S2 in the ESI†), the NR consists of only Cd and Se elements with an atomic ratio of about 1 : 1, consistent with the stoichiometric ratio of CdSe.

Although other poor metal nanoparticles such as indium and aluminum can induce clear localized surface plasmon resonance (LSPR) as well, these materials are not suitable for device optimization as their LSPR bands do not match with the bandgap of the CdSe NRs. To unveil the optical properties of the as-fabricated CuNPs, theoretical simulations based on the finite element method (FEM) were carried out using COMSOL. The red curve in Fig. 2(a) shows the simulated absorption spectrum of CuNPs with an edge length of 145 nm and a thickness of 12 nm. It is seen that the CuNPs exhibit an obvious light absorption in the range of 700 to 900 nm, with an absorption peak at around 780 nm. This theoretical result attributable to the LSPR (dipole resonance) band of the CuNPs is slightly close to the experimental absorption, in which the strongest peak is located at 760 nm.[21] In fact, the induction of the LSPR is also confirmed by electric field distribution of the CuNP array under irradiation with different wavelengths of 500, 780 and 900 nm. As shown in Fig. 2(b), once the CuNPs were irradiated by 500 nm light, no obvious hot spots (area with strong electric field density) were observed. When the wavelength was increased to 780 nm, large-area hot spots with the strongest dipolar electric energy were observed [Fig. 2(c)]. A further increase of the irradiation, however, leads to relatively weak enhancement in energy [Fig. 2(d)]. Undoubtedly, such excitation selectivity is in good agreement with the peak sensitivity at 780 nm.

As a matter of fact, the plasmonic characteristics of the present CuNPs were largely dependent on both the thickness and the edge length of the CuNPs, which has been previously observed in not only CuNPs, but also other NPs based on NM.[22,23] Fig. 3(a) shows the simulated spectra for the absorption of CuNPs with different thicknesses. For comparison, the corresponding 2D electric field energy distributions of three points

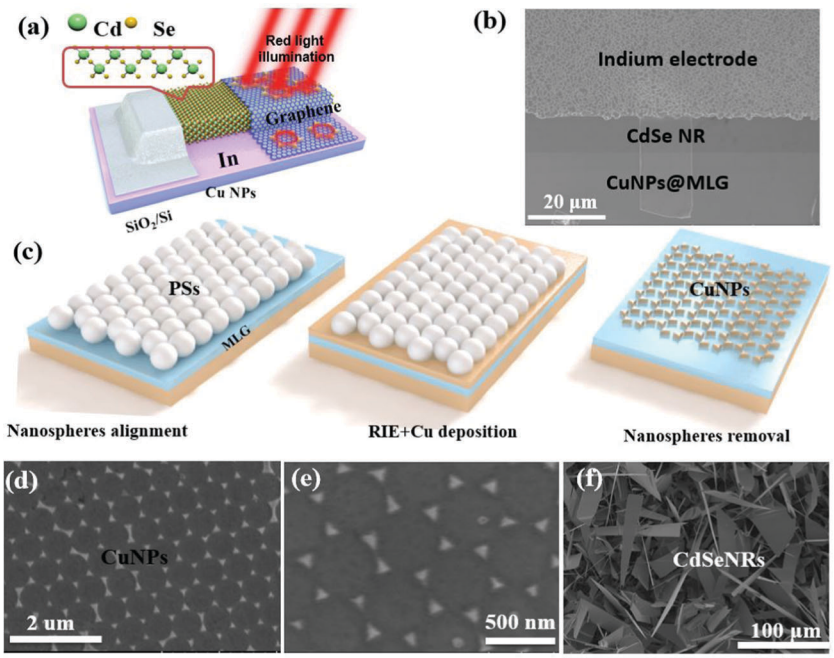

Fig. 1 (a) Schematic illustration of the nano-photodetector based on the CuNP@MLG/CdSeNR Schottky junction. (b) SEM image of the plasmonic device. (c) Schematic illustration of the step-wise process for the fabrication of the CuNP array. (d and e) Low- and high-magnification SEM images of the hexagonal CuNP array, respectively. (f) SEM image of the CdSeNRs.

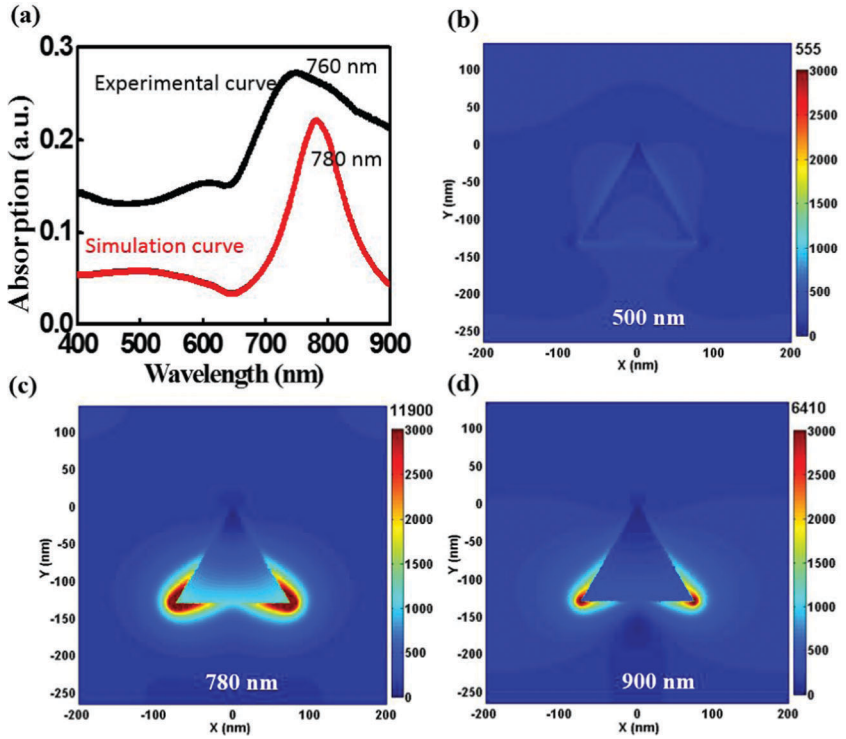

Fig. 2 (a) Theoretical and experimental absorption curves of the triangle-like CuNPs; the thickness and the side length of the CuNPs are about 12 nm and 145 nm, respectively. The CuNPs were obtained by using 500 nm PS spheres as the mask. (b–d) Electric field energy-density distribution of the CuNPs under illumination with wavelengths of 500, 780, and 900 nm.

labeled by "i", "ii", and "iii" were provided as well. It can be seen that although the enhancement of energy for all the three samples is nearly similar, the decrease of CuNP thickness however can cause noticeable red-shifts of the resonance wavelength. The strongest electric field corresponds to a thickness of ~12 nm, and a further increase or decrease of the thickness will lead to weakened electric field intensity. Notably, the weak and wide plasmonic band at around 500 nm should be associated with the multiple mode at short wavelengths.[24] In addition to thickness, the side length of the CuNPs can influence the LSPR band as well. Fig. 3(b) shows the absorption spectra of CuNPs with three different edge lengths (100, 120, and 200 nm). Apparently, the dipole peak was observed to red shift with increasing edge length of CuNPs [Fig. 3(d)]. According to further electric field distributions of CuNPs in Fig. 3(d), one can see that the highest electric field intensity corresponds to the CuNPs with an edge length of 150 nm, and other length values will lead to relatively weak electric field intensity. Considering the consistency of both the LSPR spectrum of the CuNPs and the band gap of the CdSe NR (1.7 eV), which is a necessity for plasmonic optoelectronic devices, the thickness and the edge length of the CuNPs used for assembling the plasmonic device were maintained at 12 and 145 nm, respectively.

The *I–V* curves of the MLG/CdSeNR Schottky junction in the dark were studied at room temperature, which exhibits typical rectifying characteristics. Considering the excellent contact between CdSe/indium,[25] and MLG/silver (Fig. S3, ESI†), the above rectification behavior can be ascribed to the formation of the MLG/CdSeNR Schottky junction.[26,27] The turn-on voltage is estimated to be −1.5 V, as indicated by the inset of Fig. 4(a). When illuminated by 780 nm light, the current of the as-assembled Schottky junction at negative bias voltage will be substantially increased, while the current at forward bias voltage remains virtually unchanged, indicating that the present nanostructure can function as a red light photodiode. This sensitivity at 780 nm is consistent with the absorption curve of the CdSeNRs (see Fig. S4, ESI†), and is probably related to the defect level formed during high-temperature growth. In fact, a similar finding was also observed when the MLG/CdSeNR Schottky junction was decorated with plasmonic CuNPs [Fig. 4(b)]. At a bias voltage of −3 V, the CuNP@MLG/CdSeNR device has a photocurrent of 3.1 μA, which is nearly 24 times larger than that of MLG/CdSeNRs (0.124 μA). In order to explore the effect of the plasmonic CuNPs on the optoelectronic properties of the MLG/CdSeNR, the photoresponse of both devices under repeatable 780 nm light illumination at the same bias voltage was studied. As shown in Fig. 4(c), the current of both devices can be reversibly switched between low- and high-conduction states with good reproducibility. Comparatively, the on/off ratio of the CuNP@MLG/CdSeNR device is around 1.65×10^6, which is 112 times larger than that of the unmodified device (1.45×10^4). As we discuss later, this increase in on/off ratio probably stems from the LSPR induced energetic electron injection process.

Apart from the increase in on/off ratio, the functionalization of the plasmonic CuNPs is also beneficial to response speed. Fig. 4(d) shows the repeatable switching of the CuNP@MLG/CdSeNR device

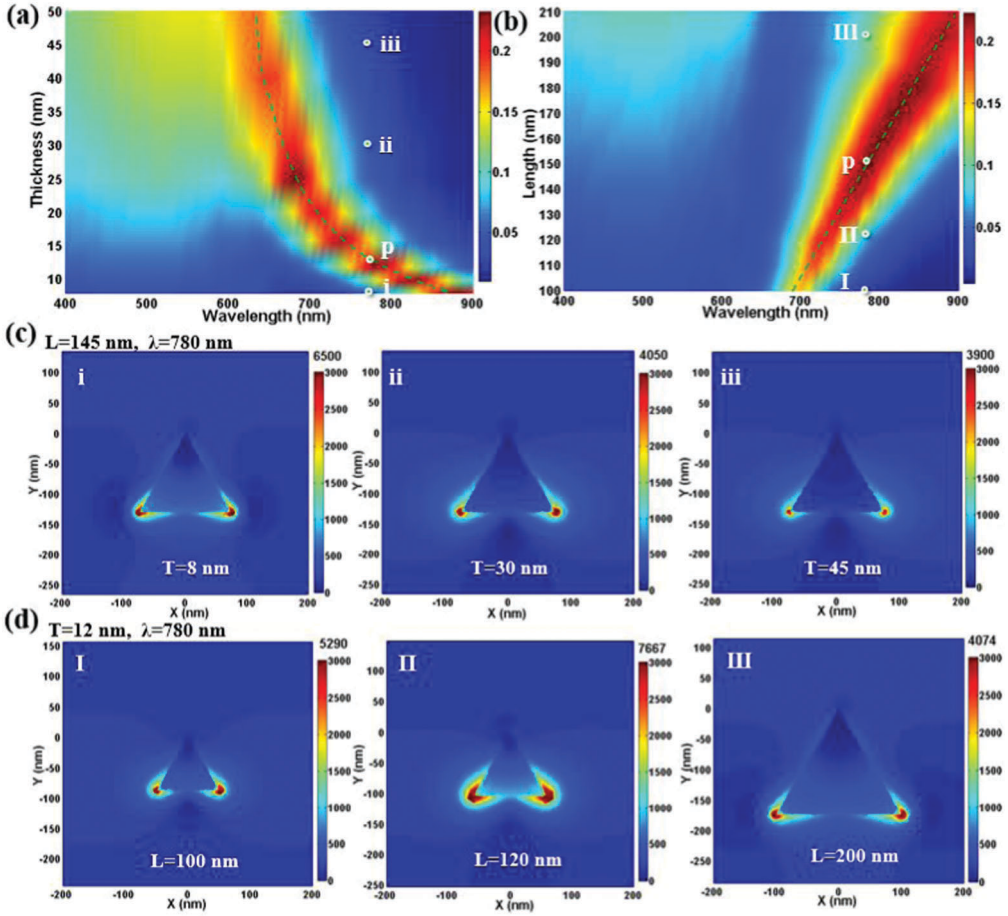

Fig. 3 The absorption intensity distribution of the CuNPs with different thicknesses (a) and different side lengths (b). The point of "p" (L = 145 nm and T = 12 nm) is provided as well. (c) The electric field distributions of CuNPs with thicknesses of 8, 30, and 45 nm, corresponding to the i, ii, and iii points shown in (a). (d) The electric field distributions of CuNPs with lengths of 100, 120, and 200 nm, corresponding to the I, II, and III points shown in (b); the simulation result in (c and d) was obtained using 780 nm light illumination.

between the "on" and "off" state when the red light was switched on and off alternatively. It is clear that the response is very fast even if the frequency is as high as 9 kHz [Fig. 4(e)], signifying that the device is capable of sensing fast-switching optical signals. From the normalized response cycle shown in Fig. 4(f), the rise/decay time (the duration needed for photocurrent to increase from 10 to 90% of the maximum or *vice versa* is defined as the rise or decay time, respectively) of the CuNP@MLG/CdSeNR photodetector is estimated to be 30/53 μs, respectively, which is about one order of magnitude faster than that of the MLG/CdSeNR device (0.19/0.31 ms, see Fig. S5, ESI†). Such a fast response rate can be attributed to the following two reasons: firstly, the high quality of the CdSeNR. In this study, the CdSeNRs synthesized by the thermal evaporation method were characterized by superior crystal quality with few defects.[28] As a result, the density of the traps was drastically reduced, which was instrumental to the fast achievement of the steady state during photodetection; secondly, the effect of LSPR. As observed in other noble metal nanoparticle enhanced nanodevices,[29,30] the response speed is substantially increased upon decoration of plasmonic nanoparticles. The detailed origin is unclear to us and needs further investigation.

It is worth pointing out that the photocurrent of the present device was also dependent on the red light intensity. Fig. 5(a) shows the I–V curves of the CuNP@MLG/CdSeNR nanodevice at different light intensities ranging from 7.65 μW cm^{-2} to 48.3 mW cm^{-2}, in which the photocurrent is found to increase with increasing light intensity. Such a light intensity dependent photocurrent is understandable in that more carriers will be generated in the device under high-intensity light illumination, leading to more electron–hole pairs separated at the MLG–CdSeNR interface and therefore a large photocurrent in the circuit. Fig. 5(b) displays the photoresponse of the device when shined by red light irradiation. The plasmonic device can be repeatedly switched on and off in the cases of both weak and strong light illumination. What is more, a simple power law ($I = CP^{\theta}$, where C is a constant, θ is the exponent that can determine the response rate, and P is the light power) can be used to describe the relationship between the photocurrent. By fitting the experimental curves to the above equation in Fig. 5(c), θ is estimated to be 0.95. Considering the fact that the exponent is highly dependent on the trapping states in the device, and that the more the exponent is close to 1, the higher quality the device will be,[31,32] we believe that the present

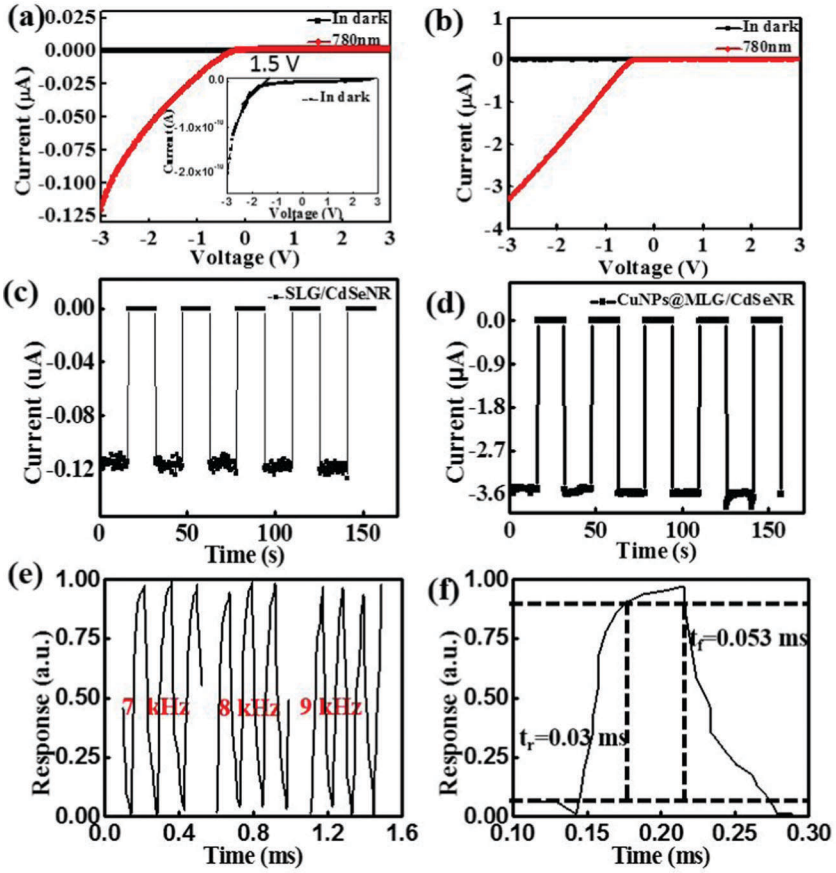

Fig. 4 (a) *I*–*V* curves of the MLG/CdSeNR Schottky junction in the dark and under light illumination; the inset shows the *I*–*V* curves at a logarithmic scale. (b) *I*–*V* curves of CuNP@MLG/CdSeNRs in the dark and under light illumination. (c and d) Photoresponse of both MLG/CdSeNR and CuNP@MLG/CdSeNR devices. (e) Photoresponse of the CuNP-modified nano-detector to switchable red light irradiation with frequencies of 7, 8 and 9 kHz. (f) Rising and falling edges for determining τ_r and τ_f of the PD after decoration with the CuNP array.

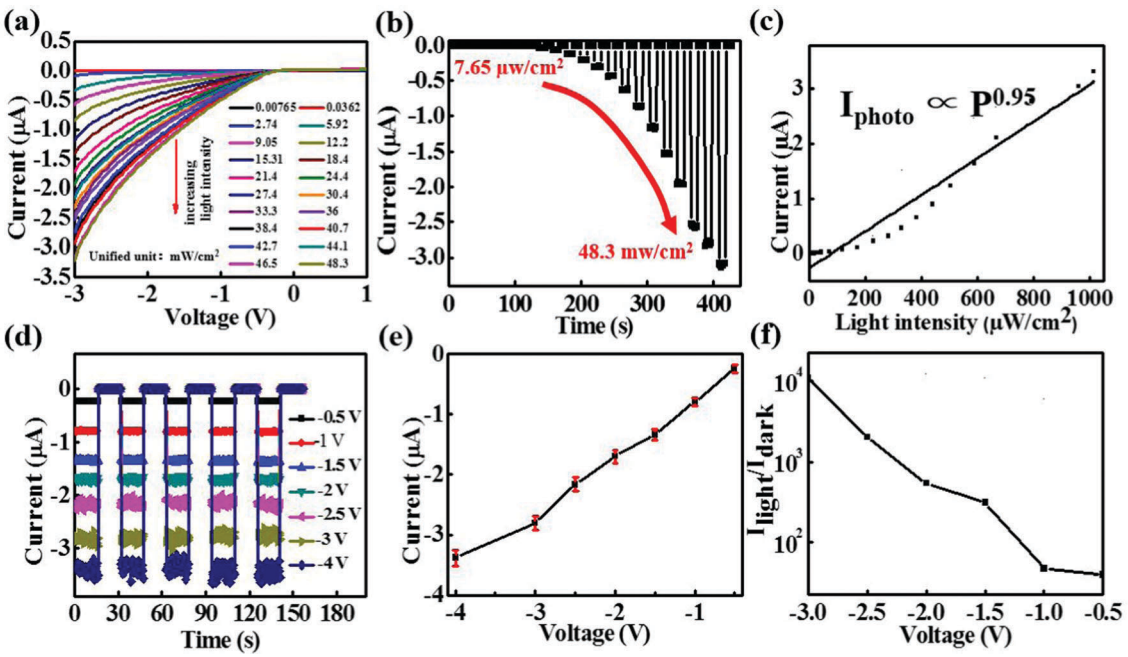

Fig. 5 (a) *I*–*V* characteristics of the CuNP@MLG/CdSeNR Schottky junction PD under the 780 nm irradiation with different intensities. (b) The corresponding photoresponse of the nanodevice. (c) Current as a function of light intensity. (d) Photoresponse switching behavior at varying voltages from −4 to −0.5 V. (e) Photocurrent as a function of bias voltage ranging from −4 to −0.5 V. (f) I_{light}/I_{dark} as a function of bias voltage.

plasmonic nano-photodetector is of high quality with a low amount of trapping states.[33] Besides, the bias voltage can influence the photocurrent of the nano-photodetector as well. Fig. 5(d) shows the photoresponse under bias voltage in the range of −4 to 0.5 V. It is easy to find that with the increase of bias voltage, the photocurrent increases accordingly [Fig. 5(e)]. Further analysis of the bias voltage dependent on/off ratio reveals a similar variation tendency, as shown in Fig. 5(f). Such a variation is reasonable as an increase in bias voltage can cause not only increased probability of carrier separation and acceleration, but also an enhanced electric field, which will be highly beneficial for the photo-generation of more carriers, and therefore it will lead to a higher photocurrent.

Next, in order to quantitatively study the effect of plasmonic CuNPs on the performance of the MLG/CdSeNR device, and clearly compare the performance of our device with those of other nanophotodetectors based on CdSe nanostructures, three most representative metrics including responsivity (R), photoconductive gain (G) and detectivity (D^*) were calculated by using the following equations:[34]

$$R = \frac{I_p}{P_{opt}} \quad (1)$$

$$G = R \cdot \left(\frac{hc}{q\lambda}\right) \cdot \frac{1}{\eta} \quad (2)$$

$$D^* = \frac{1}{NEP} \approx \sqrt{\frac{A}{2qI_d}} \cdot R \quad (3)$$

where I_p is the photocurrent (3.3×10^{-6} A), P_{opt} is the incident light power which can be calculated to be 1.938×10^{-8} W ($P_{opt} = I_{light} \times A = 32.3$ mW cm$^{-2} \times 60$ μm^2), h is Planck's constant (6.625×10^{-34} J s), c is the light speed (3×10^8 m s^{-1}), q is the elementary charge (1.6×10^{-19} C), λ is the incident light wavelength (780 nm), η is the quantum efficiency (≈ 1), and A and I_d are the PD area (60 μm^2) and the dark current (2×10^{-12} A). Based on the above values and eqn (1), the responsivity is estimated to be 170 A W^{-1}. What is more, by assuming $\eta = 1$ for convenience, the photoconductive gain and detectivity are determined to be 271 and 1.65×10^{14} cm Hz$^{1/2}$ W^{-1}, respectively. We have also studied the photoresponse of plasmonic CuNP decorated nano-photodetectors after long-term storage. Fig. S6 (ESI†) shows the photoresponse of a representative device from which we can see clearly that after storage for 2 months, the device can keep 80% of its initial photocurrent. In addition, after several cycles of repeatable switching of incident light illumination, the device still displayed obvious photostability. What is more, we may conclude that the introduction of CuNPs leads to obvious degradation in stability. Such a degradation in photosensitivity is probably related to the oxidation of CuNPs when exposed to ambient conditions.

To gain more insight into the optoelectronic properties, the responsivity of both devices in visible to near infrared light ranges (from 580–850 nm) was measured and is shown in Fig. 6. It is visible that both the MLG/CdSeNR and CuNP@MLG/CdSeNR devices exhibit good spectral selectivity. That is, they were poorly

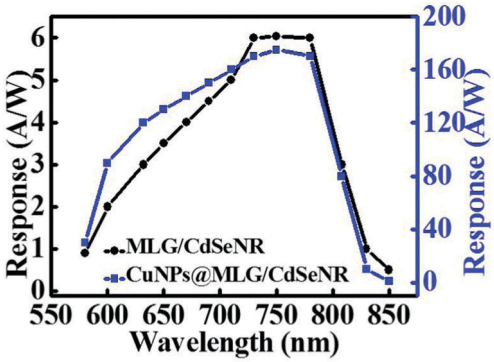

Fig. 6 Comparison of the spectral response of the red light photodetectors before and after decoration with the plasmonic CuNP array.

sensitive to irradiation with a wavelength of less than 730 nm, or larger than 780 nm, but were highly sensitive to photons with wavelength in the range of 730 to 780 nm. The peak sensitivity is at around 760 nm, which corresponds to both the LSPR band of the plasmonic CuNPs and the band-gap of CdSeNRs (1.7 eV). This coincidence in energy is related to the operation mechanism of the plasmonic red light nano-PD.

The operation mechanism of the CuNP@MLG/CdSeNR red light nanophotodetector can be interpreted by the energy band diagram shown in Fig. 7. Owing to the distinction of the work function between graphene (~4.66 eV) and CdSe (~4.2 eV), electrons will flow from CdSeNRs to graphene, leading to upward band bending of CdSeNRs near graphene, and the formation of a built-in electric field (also known as the "space charge region") with a direction pointing from CdSeNRs to graphene. When illuminated by red light, the as-formed built-in electric field was able to separate the photo-excited electron–hole pairs, forming photocurrent in the external circuit, which corresponds to the photosensing of MLG/CdSeNRs without CuNP decoration. It should be noted that this photoelectric process can be strengthened once a large number of CuNPs with strong LSPR were coated onto the MLG surface. Under such a circumstance, in addition to the contribution from the MLG/CdSeNR heterojunction,

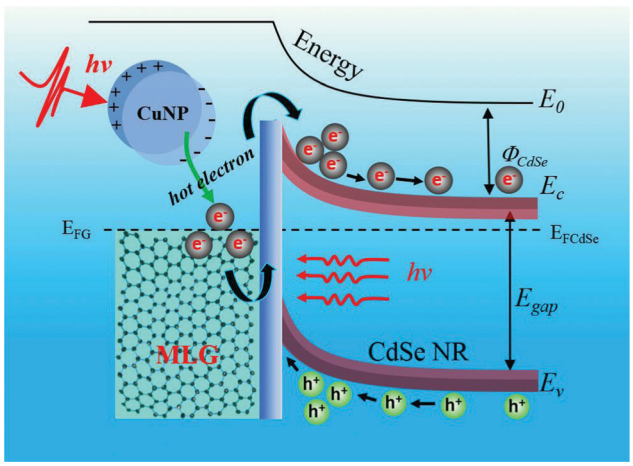

Fig. 7 Energy band diagram of the plasmonic red light nano-PD.

the photocurrent will enjoy an extra increase which is related to the plasmonic CuNP-mediated energetic electron injection mechanism. Like other plasmonic noble metal nanoparticles,[35,36] when irradiated by 780 nm light, the electrons in CuNPs will witness a strong collective oscillation. As a result, the hot energy with energy as high as 4 eV[37] can readily inject to neighboring MLG. These electrons can then migrate to the MLG–CdSeNR contact, and swept by the built-in electric field to contribute to photocurrent in the external circuit.

3. Conclusions

In this study, we present a plasmonic CuNP array induced sensitive MLG–CdSeNR Schottky junction red light photodetector. The CuNPs exhibit obvious LSPR which is highly dependent on their size. Photoelectric analysis showed that after decoration with CuNPs, the photocurrent increased by about 24 times, from 0.124 to 3.1 μA. In addition, other device parameters including responsivity and gain were considerably enhanced. Such an optimization in device performance, according to theoretical modeling based FEM, was related to the contribution from LSPR mediated direct hot electron injection. This study shows that plasmonic CuNP arrays are promising candidates for improving the performance of optoelectronic devices.

4. Experimental section

Synthesis and characterization of CdSeNRs and CuNP@MLG

The MLG film was synthesized *via* a Cu-catalyzed chemical vapor deposition (CVD) method at 1000 °C using a mixed gas of CH_4 (40 SCCM) and H_2 (20 SCCM) as precursors. After growth, the MLG layers were coated with polymethylmethacrylate (PMMA) through spin-coating, and the catalytic Cu foil was removed using an etch solution ($CuSO_4$: HCl : H_2O = 10 g : 50 ml : 50 ml). To fabricate the CuNP array@MLG nanostructures, hexagonal monolayer polystyrene (PS) spheres (diameter: 500 nm) were firstly self-assembled onto a MLG film by the drop-coating process. Then, a 12 nm thick copper nanofilm was deposited on the closely packed PS spheres by thermal evaporation, followed by the removal of the PS spheres in a xylene solution for 24 h. The CdSeNRs were fabricated by thermally evaporating pure CdSe powder at 900 °C in a horizontal tube furnace *via* a conventional vapor–liquid–solid (VLS) process, in which Au-coated silicon substrates at the downstream position about 10 cm away from the CdSe powder were used as catalysts. Briefly, the tube furnace was evacuated to a base pressure of 10^{-3} Pa, and then backfilled with a constant Ar and H_2 (5%) gas flow of 30 SCCM to a pressure of ~250 Pa. Afterwards, the CdSe source was heated up to 900 °C at a rate of 18 °C min^{-1} and the temperature was maintained for 2 h. After growth, the furnace was naturally cooled down to ambient temperature and the Si substrate containing the black wool-like product was collected. The morphology of the hexagonal CuNP arrays and CdSeNRs was characterized using a field-emission scanning electron microscope (FESEM, SIRION 200 FEG), equipped with an EDS analyzer. The MLG was analyzed using a Raman spectrometer (JY, LabRAM HR800).

Device fabrication and characterization

To fabricate the plasmonic photodetector, photolithography and thermal evaporation were employed to define the indium electrode (100 nm) on single CdSeNR which was dispersed on a SiO_2 (300 nm-thick)/Si substrate in a parallel fashion by a contact printing approach.[37] The remaining photoresist was removed by a simple lift-off process. A MLG film decorated with a hexagonal CuNP array was then transferred onto the other head of the CdSeNR. Afterwards, silver paste was placed onto the MLG. The optoelectronic characteristics of the plasmonic photodetector were investigated at room temperature using a homebuilt setup composed of an *I–V* semiconductor characterization system (Keithley 4200-SCS) and a monochromatic light source system. 780 nm light was provided by a commercial laser diode (Thorlabs Comp., L780P010), which was mounted on a Laser Diode Mount (Thorlabs Comp., TCLDM9). To study the response speed of the nanodevice at high frequency, a lock-in amplifier (Stanford Research Systems, Model SR830 DSP) was introduced into the above setup.

Theoretical simulations

The theoretical results were calculated by using the finite element method (FEM) to study a unit cell (400 nm × 400 nm) of the model. The size of the nanoparticles in the model is set to be identical to that obtained from the corresponding SEM image. The permittivity of Cu and CdSe in this calculation was obtained from Sopra S.A. Company database. The periodic boundary conditions are employed for the corresponding lateral boundaries in *x* and *y* directions of the simulation model. The perfectly matching layers (PMLs) were utilized at the calculated region boundaries to reduce the influence of light reflection. The transverse magnetic (TM) polarized light was assumed to be normally incident from the top of the structure (the electric field parallels with the bottom edge of the CuNPs).

Acknowledgements

This work was supported by the Natural Science Foundation of China (NSFC, No. 61575059 and 61675062) and the Fundamental Research Funds for the Central Universities (2012HGCX0003, 2013HGCH0012, and 2014HGCH0005).

References

1 S. A. Maier, M. L. Brongersma, P. G. Kik, S. Meltzer, A. A. G. Requicha and H. A. Atwater, *Adv. Mater.*, 2001, **13**, 1501.
2 Q. Zhang, Y. X. Hu, S. R. Guo, J. Goebl and Y. D. Yin, *Nano Lett.*, 2010, **10**, 5037.
3 C. B. Gao, J. Geobl and Y. D. Yin, *J. Mater. Chem. C*, 2013, **1**, 3898.
4 Q. Zhang, J. P. Ge, T. Pham, J. Goebl, Y. X. Hu, Z. G. Lu and Y. D. Yin, *Angew. Chem., Int. Ed.*, 2009, **48**, 3516.
5 L. W. Jang, D. W. Jeon, M. Kim, J. W. Jeon, A. Y. Polyakov, J. W. Ju, S. J. Lee, J. H. Baek, J. K. Yang and I. H. Lee, *Adv. Funct. Mater.*, 2012, **22**, 2728.

6 Y. Wang, C. W. Ge, Y. F. Zou, R. Lu, K. Zheng, T. F. Zhang, Y. Q. Yu and L. B. Luo, *Adv. Opt. Mater.*, 2016, **4**, 291.
7 M. W. Knight, H. Sobhani, P. Nordlander and N. J. Halas, *Science*, 2011, **332**, 702.
8 X. Wu, E. S. Thrall, H. Liu, M. Steigerwald and L. Brus, *J. Phys. Chem. C*, 2010, **114**, 12896.
9 F. J. Beck, T. Lasanta and G. Konstantatos, *Adv. Opt. Mater.*, 2014, **2**, 493.
10 H. A. Atwater and A. Polman, *Nat. Mater.*, 2010, **9**, 205.
11 L. B. Luo, K. Zheng, C. W. Ge, Y. F. Zou, R. Lu, Y. Wang, D. D. Wang, T. F. Zhang and F. X. Liang, *Plasmonics*, 2016, **11**, 619.
12 J. S. Miao, W. D. Hu, N. Guo, Z. Y. Lu, X. Q. Liu, L. Liao, P. P. Chen, T. Jiang, S. W. Wu, J. C. Ho, L. Wang, X. S. Chen and W. Lu, *Small*, 2015, **11**, 936.
13 R. F. Oulton, V. J. Sorger, D. A. Genov, D. F. P. Pile and X. Zhang, *Nat. Photonics*, 2008, **2**, 496.
14 J. F. Lu, C. X. Xu, J. Dai, J. T. Li, Y. Y. Wang, Y. Lin and P. L. Li, *Nanoscale*, 2015, **7**, 3396.
15 G. H. Chan, J. Zhao, E. M. Hicks, G. C. Schatz and R. P. Van Duyne, *Nano Lett.*, 2007, **7**, 1947.
16 K. L. Kelly, E. Coronado, L. L. Zhao and G. C. Schatz, *J. Phys. Chem. B*, 2003, **107**, 668.
17 S. B. Wang, R. S. Chen, S. J. Chang, H. C. Han, M. S. Hu, K. H. Chen and L. C. Chen, *Nanoscale*, 2013, **6**, 1264.
18 M. A. Nazirzadeh, F. B. Ater, B. B. Turgut and A. K. Okyay, *Sci. Rep.*, 2014, **4**, 7103.
19 J. S. Miao, W. D. Hu, Y. L. Jing, W. J. Luo, L. Liao, A. L. Pan, S. W. Wu, J. X. Cheng, X. S. Chen and W. Lu, *Small*, 2015, **11**, 2392.
20 W. Y. Kong, G. A. Wu, K. Y. Wang, T. F. Zhang, Y. F. Zou, D. D. Wang and L. B. Luo, *Adv. Mater.*, 2016, **28**, 10725.
21 Q. Zhang, D. Q. Lima, I. Lee, F. Zaera, M. Chi and Y. Yin, *Angew. Chem., Int. Ed.*, 2011, **50**, 7088.
22 G. H. Chan, J. Zhao, E. M. Hicks, G. C. Schatz and R. P. V. Duyne, *Nano Lett.*, 2007, **7**, 1947.
23 Y. Yang, S. Matsubara, M. Nogami, J. L. Shi and W. M. Huang, *Nanotechnology*, 2006, **17**, 2821.
24 M. Rang, A. C. Jones, F. Zhou, Z. Y. Li, B. J. Wiley, Y. Xia and M. B. Raschke, *Nano Lett.*, 2008, **8**, 3357.
25 L. B. Luo, W. J. Xie, Y. F. Zou, Y. Q. Yu, F. X. Liang, Z. J. Huang and K. Y. Zhou, *Opt. Express*, 2015, **23**, 12979.
26 X. Li, H. Zhu, K. Wang, A. Cao, J. Wei, C. Li, Y. Jia, Z. Li, X. Li and D. Wu, *Adv. Mater.*, 2010, **22**, 2743.
27 J. H. Werner, *Appl. Phys. A: Mater. Sci. Process.*, 1988, **47**, 291.
28 J. S. Jie, W. J. Zhang, Y. Jiang, X. M. Meng, Y. Q. Li and S. T. Lee, *Nano Lett.*, 2006, **6**, 1887.
29 K. W. Liu, M. Sakurai, M. Y. Liao and M. Aono, *J. Phys. Chem. C*, 2010, **114**, 19835.
30 L. B. Luo, X. L. Huang, M. Z. Wang, C. Xie, C. Y. Wu, J. G. Hu, L. Wang and J. A. Huang, *Small*, 2014, **10**, 2645.
31 N. V. Joshi, *Marcel Dekker*, New York, 1990.
32 A. Rose, *Interscience*, New York, 1963.
33 H. Kind, H. Yan, B. Messer, M. Law and P. Yang, *Adv. Mater.*, 2002, **14**, 158.
34 F. Wang, Z. Wang, Q. Wang, F. Wang, L. Yin, K. Xu, Y. Huang and J. He, *Nanotechnology*, 2015, **26**, 292001.
35 S. Linic, P. Christopher and D. B. Ingram, *Nat. Mater.*, 2011, **10**, 911.
36 M. Lee, J. U. Kim, J. S. Lee, B. I. Lee, J. Shin and C. B. Park, *Adv. Mater.*, 2014, **26**, 4463.
37 B. Nie, L. B. Luo, J. J. Chen, J. G. Hu, C. Y. Wu, L. Wang, Y. Q. Yu, Z. F. Zhu and J. S. Jie, *Nanotechnology*, 2013, **24**, 095603.